ACS APPLIED MATERIALS & INTERFACES

Research Article

www.acsami.org

Subeutectic Growth of Single-Crystal Silicon Nanowires Grown on and Wrapped with Graphene Nanosheets: High-Performance Anode Material for Lithium-Ion Battery

Fathy M Hassan,[†] Abdel Rahman Elsayed,[†] Victor Chabot,[†] Rasim Batmaz,[†] Xingcheng Xiao,*[,‡] and Zhongwei Chen*[,†]

[†]Department of Chemical Engineering, University of Waterloo, Ontario, Canada N2L3G1

[‡]Chemical Sciences and Materials Systems, General Motors Global Research and Development Center, Warren, Michigan 48090, United States

Supporting Information

ABSTRACT: A novel one-pot synthesis for the subeutectic growth of (111) oriented Si nanowires on an in situ formed nickel nanoparticle catalyst prepared from an inexpensive nickel nitrate precursor is developed. Additionally, anchoring the nickel nanoparticles to a simultaneously reduced graphene oxide support created synergy between the individual components of the c-SiNW-G composite, which greatly improved the reversible charge capacity and it is retention at high current density when applied as an anode for a Li-ion battery. The c-SiNW-G electrodes for Li-ion battery achieved excellent high-rate performance, producing a stable reversible capacity of 550 mAh g^{-1} after 100 cycles at 6.8 A g^{-1} (78% of that at 0.1 A g^{-1}). Thus, with further development this process creates an important building block for a new wave of low-cost silicon nanowire materials and a promising avenue for high rate Li-ion batteries.

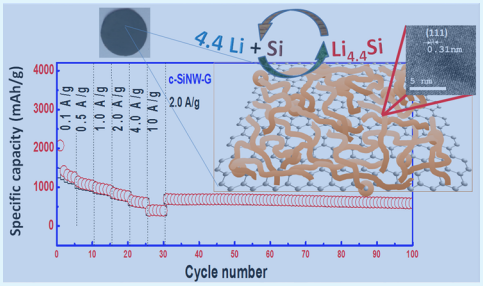

KEYWORDS: *nanostructured catalyst, silicon nanowires, lithium-ion battery, graphene, rate capability, electrochemical performance*

INTRODUCTION

The development of lithium-ion batteries (LIB) based on new high-performance materials is critical to meet the demands of an expanding array of mobile consumer and military electronics that incorporate this technology. Advances in the energy storage capabilities of LIBs are also integral to the future of electric transportation and grid scale energy storage required to facilitate the integration of intermittent renewable energy sources into the grid. Specifically, alternative electrode technologies are needed to overcome the maximum theoretical capacity (372 mAh g^{-1}) of graphite anode materials and their poor capacity retention at high current density.[1−6] Silicon (Si) has emerged as a strong candidate for the future of commercial LIB anode designs because of its high theoretical storage capacity in comparison to graphite (4200 mAh g^{-1}), natural abundance, low cost, and low discharge potential of 0−0.4 V vs Li/Li^+.[7−11]

Unfortunately, the commercial application of silicon-based anodes faces several challenges that arise due to its low intrinsic electrical conductivity (1×10^{-5} S cm^{-1}), along with extreme volume expansion (400%) that occur during the alloying process with lithium ($Li_{4.4}Si$). These volume expansions inevitably lead to pulverization of the electrolyte and/or rapidly degrading electrical connectivity of the electrode, especially when using electrodes with high mass loadings.[12−17] Furthermore, the intense lattice strain and surface stress can prevent stabilization of the solid electrolyte interphase layer (SEI), leading to low columbic efficiency. In efforts to overcome these challenges, various conductive-carbon composite materials have been utilized to encapsulate the silicon materials, thereby enhancing their performance retention after many cycles.[18−27] Additionally, tailored nanostructures, such as Si nanowires (SiNWs), nanotubes or nanoporous structures have been used to achieve better durability through a combination of increased strain tolerance, shorter diffusion distances and enhanced charge transport.[28−37]

In this regard, there is an evolving array of methods used for both the bottom-up and top-down growth of SiNWs that have been successfully demonstrated on planar Si surfaces.[38,39] However, the commonly utilized bottom-up method for SiNWs growth is the vapor−liquid−solid (VLS) catalytic growth mechanism, using gold (Au) nanoparticles that are chosen for their relatively low eutectic point.[40−42] In addition to the aligned vertical growth SiNWs being demonstrated on Si(111) wafers using the VLS approach, SiNWs have also been grown on other substrates, such as Al_2O_3.[43,44] Practical safety risks of the commonly used SiH_4 gas precursors and the high cost of Au are, however, a major drawback to these methods. Additionally, the production capabilities are also limited due to the requirement of using well-defined 2D planar surfaces as the

Received: May 22, 2014
Accepted: July 31, 2014
Published: July 31, 2014

   dx.doi.org/10.1021/am5032067 | ACS Appl. Mater. Interfaces 2014, 6, 13757−13764

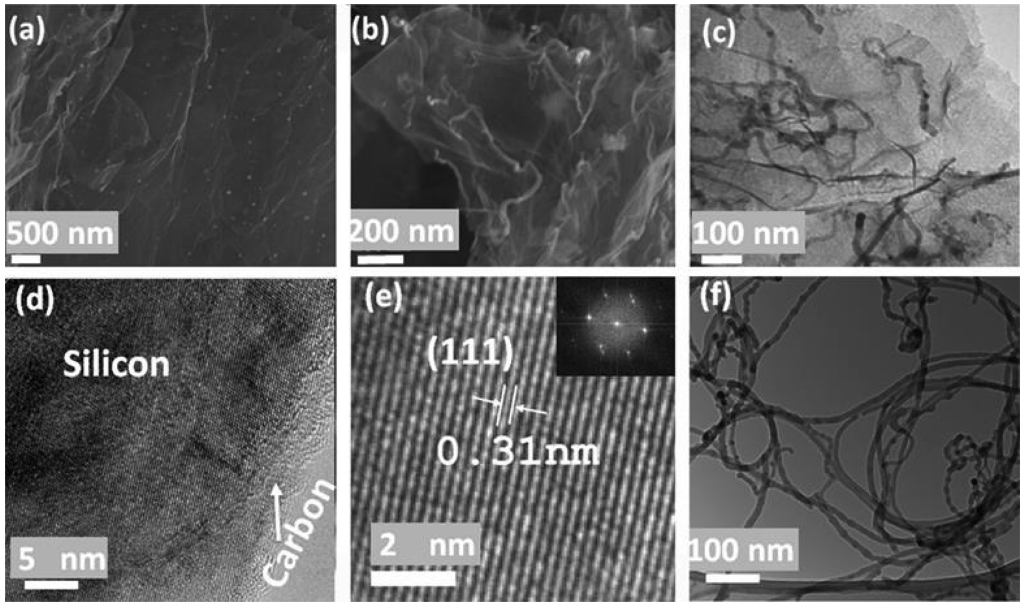

Figure 1. SEM images of (a) Ni nanoparticles formed on graphene after thermal shock reduction of the nickel nitrate and GO mixture and (b) the resulting SiNWs grown on the intermediate in a. (c) TEM image of the c-SiNW-G composite, (d) increased magnification TEM image representing the SiNWs within the c-SiNW-G composite, (e) HRTEM and a corresponding FFT diffraction pattern shown in the inset for the SiNW, and (f) the TEM image for SiNWs grown without graphene support.

growth substrate. To address this, it is recognized that new methods, which employ inexpensive catalyst metals and are applicable to bulk production of SiNWs, must be developed in order to capitalize on the highly promising application potential of these materials.[38,45−47] Recent investigations toward this goal include the growth of SiNWs on Au-coated Al_2O_3 particles,[43] and in work concurrent to our own, the VLS growth of SiNWs from Au nanoparticles on the surface of reduced graphene oxide (rGO).[45]

Herein we present a scalable method for the bottom-up processing of carbon-coated SiNWs on graphene (c-SiNW-G) using an inexpensive nickel nanoparticle (NiNP) catalyst. This procedure involves a sophisticated one-pot atmospheric pressure chemical vapor deposition (APCVD) synthesis, which incorporates several novel techniques. First, a uniform distribution of NiNPs on the surface of graphene was achieved by thermally shocking a mixture of nickel nitrate and graphene oxide, resulting in rapid decomposition of the nickel nitrate precursor and simultaneous in situ reduction of the graphene oxide. Second, the SiNWs were grown on the NiNP catalysts by applying a unique variation to the silicide-assisted vapor−solid−solid (VSS) mechanism.[38,46−48] The seed particles remained in the solid phase because of the subeutectic temperature of 900 °C,[48] well below the 993 °C eutectic temperature required for the Ni−Si system to undergo a VLS growth mechanism.[38] Furthermore, by exchanging the $SiCl_4$ precursor after SiNWs growth with toluene, we illustrate a core−shell SiNW/C structure can be obtained. In addition to the elimination of expensive Au catalysts using this method, the ability to grow SiNWs anchored on graphene using $SiCl_4$, along with the introduction of a controlled carbon coating by the injection of toluene represents a significant step toward the future development of practical high performance materials for LIBs. By growing SiNWs directly on graphene, a direct path is provided for electrical conductivity. Furthermore, by decorating the graphene sheets with well-dispersed NiNPs, it provides a template for growing individual SiNWs that are not agglomerated together.

EXPERIMENTAL METHODS

Synthesis of SiNW-G. Prior to growing SiNWs on graphene and the fabrication of well-dispersed NiNPs, graphene oxide (GO) was synthesized by a modified Hummer's method.[49] In a typical experiment, 150 mg of GO was dispersed in deionized water followed by dropwise addition of 300 μL of 0.1 M nickel nitrate hexahydrate ($Ni(NO_3)_2.6H_2O$). The mixture was sonicated for 30 min and then left to dry at 60 °C under magnetic stirring. The GO-nickel nitrate mixture was then transferred to a quartz tube inside a furnace and rapidly pushed into the hot zone at 700 °C and held under argon atmosphere for 1 h. The temperature was then increased to 900 °C and H_2 gas was purged for 30 min at 500 sccm before injecting 300 μL of $SiCl_4$ into the quartz tube. After the $SiCl_4$ was completely depleted and the SiNW-G grown, toluene was injected (typically 50 μL) as a source of the carbon coating, before cooling the furnace down. The process generated approximately 30 mg of c-SiNW-G powder containing 48 wt % SiNW.

Electrode Fabrication. Battery electrodes were fabricated by mixing the active c-SiNW-G material (70 wt %) with polyacrilonitrile (PAN, 30 wt %) and casting the slurry on a copper foil current collector. No further carbon additives were used. The electrodes were then heat treated at 550 °C for 2 h in Argon atmosphere to enhance the three-dimensional conductivity of the composite electrode by partially pyrolyzing the polyacrylontirile binder. The initial starting thickness of the electrodes were about 15 μm. The electrode remained intact and well-attached to the current collector after heat treatment. Figure S1 (in the Supporting Information) shows a digital image of the electrode before and after the heat treatment process.

Electrochemical Performance. Coin cells were assembled in an argon-filled glovebox using the treated electrodes versus metallic lithium and using 1 M LiPF6 in 30 wt % ethylene carbonate (EC), 60 wt % dimethyl carbonate (DMC), and 10 wt % fluorinated ethylene carbonate (FEC). Galvanostatic cycling was initially performed between 0.01−2 V at 100 mA g^{-1} (C/20) for 5 cycles. After initial cycling the current rate was varied: one cell remained at 100 mA g^{-1} current for 100 cycles, and another cell was cycled at incremental rates of 0.1, 0.5, 1, 2, 4, and 10 A g^{-1} to determine the rate capability of the

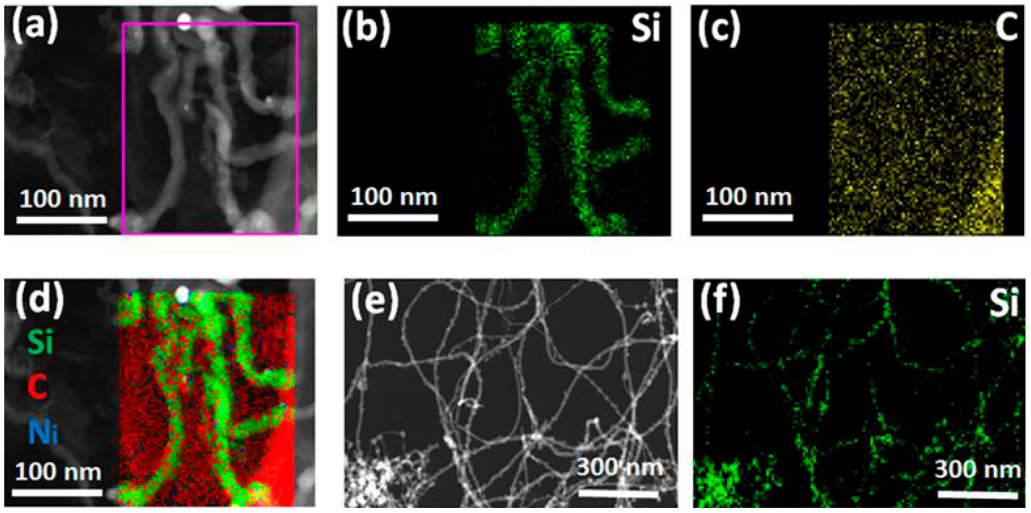

Figure 2. (a) HAADF-STEM (high-angle annular dark-field) of c-SiNW-G, (b) EDX mapping of Si for the area marked in a, (c) EDX mapping of carbon, (d) overlapping projection for the Si, C and Ni spectra measured in c-SiNW-G, (e) HAADF-STEM of SiNWs grown without graphene, and (f) the EDX mapping for Si in e.

materials. As a reference material, graphene was tested under the same conditions and electrode preparation. Cyclic voltammetry (CV) was also performed, utilizing a 0.01−2 V range. In all measurements, the total mass of the electrode, including the mass of the silicon and the mass of the graphene, was considered when carrying out capacity calculations.

Characterization. Morphology of the electrode surfaces before and after treatment were characterized by scanning electron microscopy (SEM) using a LEO FESEM 1530 and transmission electron microscopy (TEM) using a JEOL 2010F TEM/STEM field emission microscope equipped with a large solid angle for high X-ray throughput, scanning, scanning-transmission and a Gatan imaging filter (GIF) for energy filtered imaging. Raman scattering spectra were recorded on a Bruker Sentterra system (532 nm laser). Thermal gravimetric analysis (TGA) (TA Instruments Q500, USA) was used to determine the mass ratio of graphene to SiNW. TGA testing was performed in air with a temperature range of 25 to 900 °C and a ramp rate of 10 °C min^{-1}. XRD analysis was conducted using monochromatic Cu K X-rays (0.154 nm wavelength) and an Inel XRG 3000 diffractometer.

RESULTS AND DISCUSSION

To verify the production of uniformly distributed NiNPs as a catalyst for SiNW growth, we removed the samples from the furnace after the initial thermal shock to decompose and reduce the NiN/GO mixture.The SEM image in Figure 1a illustrates that small, approximately 10−20 nm NiNPs uniformly distributed across the entire surface of graphene were formed from the decomposition of the crystallized salt clusters. In Figure 1b, c, after injecting the $SiCl_4$ and later toluene, wormlike nanowires coated with carbon could be clearly observed by both SEM and TEM, respectively, lying flat along the basal plane of graphene. High-angle annular dark field (HAADF-STEM) imaging of the materials, which is very sensitive to atomic number, is shown in Figure 2a. This imaging technique creates an obvious variation in contrast which was used to probe the elemental distribution of the materials and to verify that the NiNPs do indeed catalyze and anchor the nanowire growth. Further, to prove the Si nanowire composition was not mistaken for carbon nanostructures formed during toluene injection, we additionally performed EDX mapping. The result shown in Figure 2a−d clearly depicts the presence of SiNWs anchored to the NiNP catalyst. Furthermore, the blanketed carbon in Figure 2c and amorphous region at the SiNWs edge in Figure 1d indicate successful coating of a very thin carbon layer on the SiNWs, in addition to the underlying graphene support.

High-resolution TEM imaging and the corresponding FFT spectrum for the SiNW-G composites (Figure 1d, e) reveal that the SiNWs exhibits a single crystalline structure with 0.31 nm lattice spacing. This indicates that growth is oriented along the (111) crystal plane. In agreement with a previous fundamental investigation, the rapid heat treatment of the Si source and the resulting (111) crystal orientation suggests the formation mechanism involves generation of an intermediate NiSi phase, which promotes (111) crystal growth.[46,47] Using an inexpensive Ni catalyst to control the axial orientation in the ⟨111⟩ direction also suggests an increased percentage of (110) facets, which offer increased lithium ion diffusion into the core of the SiNWs,[50] which promotes high-rate capabilities. The formation of a thin 2 nm layer of amorphous carbon on the surface of the SiNWs is also confirmed by high-resolution TEM (Figure 1d). The carbon coating is intended to provide additional electronic conductivity, protect against surface oxidation of the narrow SiNWs and partially restrict expansion due to lithiation.

To validate the proposed VSS growth mechanism on NiNPs, it is important to eliminate any concern that graphene may assist in the catalysis.[51,52] This would further help to verify the versatility of this inexpensive preparation method. To accomplish this, SiNWs were also produced without the addition of graphene oxide, by growing SiNWs using $SiCl_4$ precursor directly on bulk NiNPs after thermal decomposition of the nickel nitrate. This is illustrated by the characteristic TEM image shown in Figure 1f and the EDX mapping shown in Figure 2e, f. Bulk preparation of pure SiNWs grown by this methodology could be applied in the future toward various applications, without the need to anchor the NiNPs on a specific support material.

The structure of the c-SiNW-G composites was further investigated by XRD and Raman spectroscopy (Figure 3). As expected, the XRD (Figure 3a) patterns are consistent with a reference database pattern for the Si phase. No further residual peaks were observed in the c-SiNW-G composites that might correspond to residual nickel silicide or SiO_x. It was also

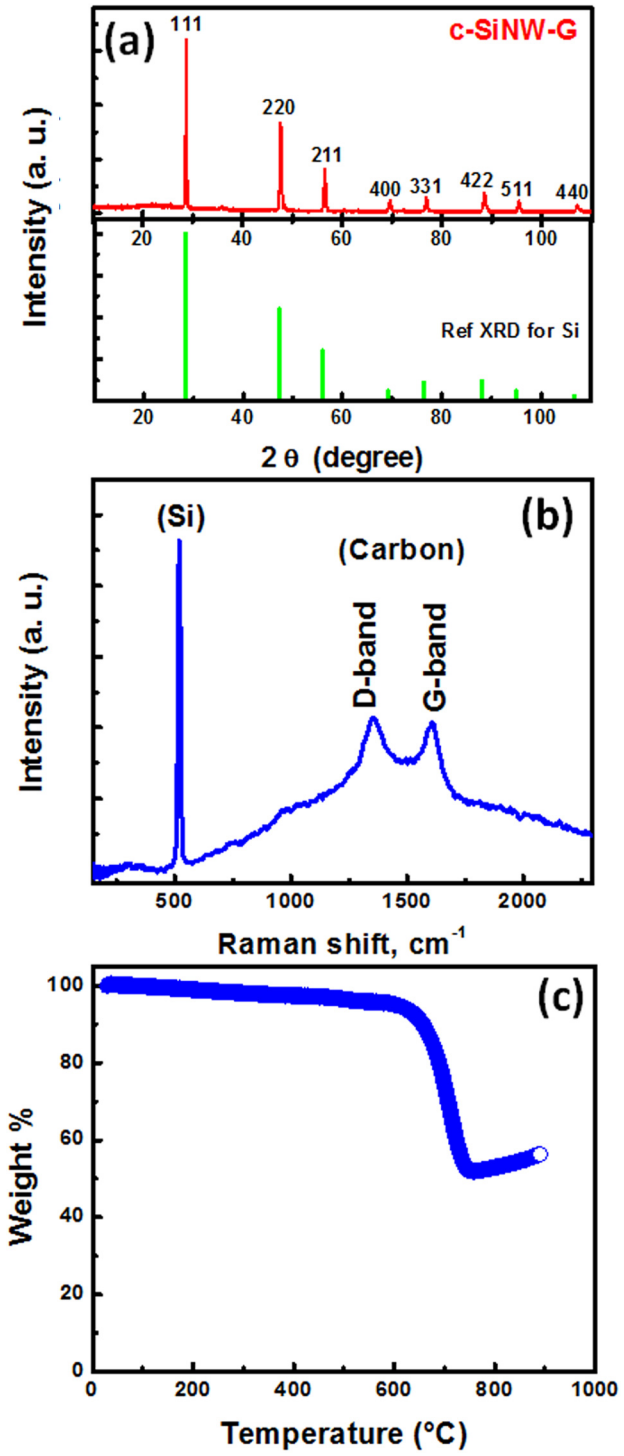

Figure 3. (a) XRD patterns for the as-synthesized c-SiNW-G (top) and the reference XRD spectrum measured for SiNP (bottom). (b) Raman spectroscopy for c-SiNW-G. (c) TGA result for c-SiNW-G.

expected that for rGO, a broad low intensity peak at ~25°, which represents a shift to the interplanar spacing interactions of graphite (002) might be observed. The absence of this peak suggests that the strong signal of the SiNWs and their presence in between the rGO sheets may suppress the weak graphitic interaction after GO reduction. However, three characteristic peaks observed in the Raman spectrum provided in Figure 3b confirm the presence of rGO after completing the one-pot synthesis. The first peak verifies the lattice vibration of crystalline Si (520 cm^{-1}), whereas the other two highlight the presence of reduced graphene oxide within the composite. The absence of Si−O−Si vibration and stretching peaks below 1000 cm^{-1} suggests minimal oxidation to the surface of the carbon-coated SiNWs during or after growth.[37,53,54] Furthermore, the strong D (~1350 cm^{-1}) and G (~1580 cm^{-1}) band peaks respectively signify a variety of planar defects and the restoration of sp^2 binding within the graphitic lattice, respectively.[55,56] Figure 3c demonstrates the TGA profile for the c-SiNW-G electrode material after annealing. As the temperature increases, a significant mass loss is observed from ca. 610 to 720 °C due to the carbon content being burned away. Following this, a mass increase is observed at higher temperature, which can be ascribed to the oxidation of silicon to silicon oxide. As a result, the Si wt % in the c-SiNW-G is about 48%.

To demonstrate the potential application of the SiNWs prepared using the inexpensive nickel catalyst, we conducted a series of investigations to determine the electrochemical performance in LIBs. The c-SiNW-G was dispersed as the active material in a slurry and deposited on a copper current collector before partially carbonizing the PAN binder. The anodes were then assembled into coin cells with a lithium counter electrode and underwent galvanostatic charge−discharge (CD) cycling, cyclic voltammetry (CV) and electrochemical impedance spectroscopy (EIS).

Figure 4a illustrates the CD voltage profile for the c-SiNW-G anodes cycled between 0.01 and 2 V @ 0.1 A g^{-1}. A large plateau in the first discharge cycle corresponds to the expected behavior of crystalline Si. Beyond the first cycle, the observed changes in the voltage profile are attributed to amorphization of the initially crystalline SiNW structure. This is supplemented by the added irreversible first cycle capacity loss of graphene (see inset in Figure S2 in the Supporting Information).[57−59] The first cycle discharge capacity is 2200 mAh g^{-1} with a Coulombic efficiency of 64%. The second cycle has a capacity of 1416 mAh g^{-1}, followed by a gradual decrease to only 931 mAh g^{-1} at the 30th cycle. However, as depicted by the cycle rate test in Figure 4c, at higher current densities up to 10 A g^{-1} the c-SiNW-G composite was remarkably still able to deliver reversible capacity of 400 mAh g^{-1}, providing sufficient electron and ion transport to support the partial lithiation reaction. Even after 70 additional cycles at 2 A g^{-1}, the c-SiNW-G composite remained highly stable (730 mAh g^{-1}). The charge−discharge profile in Figure 4d, taken from the last cycle of each rate investigated, reveals minimal variation in the shape or voltage of the plateau region below 2 A g^{-1}, although at higher current density the development of slightly increased slope and overpotential is observed. When further compared to pure graphene or pure SiNW active materials in the electrodes, there was a strong synergistic effect present for the c-SiNW-G. This synergy greatly improved capacity retention at high charge/discharge rates (~3.5× improvement at 2 A g^{-1} and ~10× at 10 A g^{-1}). To fully illustrate the rapid transport capabilities of the c-SiNW-G composite, a newly assembled cell underwent three conditioning cycles at 100 mA g^{-1} before directly cycling at a high current density of 6.8 A g^{-1}. As shown in Figure 4e, after 100 cycles, a stabilized capacity of 550 mAh g^{-1} was achieved. Figure 4b compares the cycle performance, at 0.1 A/g, for c-SiNW-G, with the noncarbon coated SiNW-G, and graphene. The figure shows that introduction of a thin carbon layer to SiNW-G significantly improves the cycle stability. Through heat-treatment of polyacrylonitrile (PAN), its

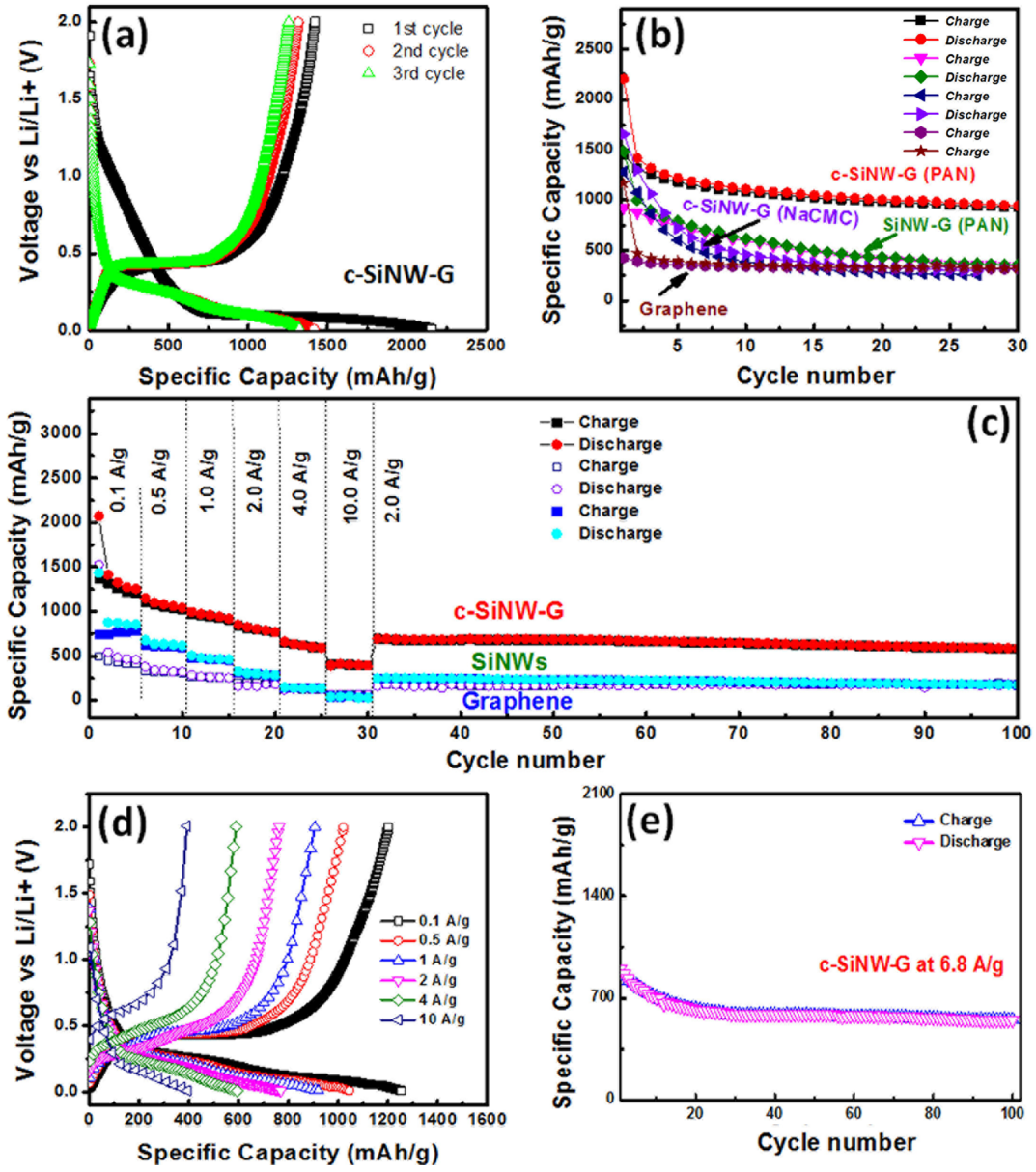

Figure 4. (a) Voltage profile for a coin cell containing c-SiNW-G cycled at 0.1 A g^{-1}, (b) comparison of the cycle capability of SiNW-G with and without carbon coating using PAN, and c-SiNW-G using NaCMC, to that of pure graphene at 0.1 A g^{-1}, (c) rate capability of SiNW-G compared to the nonsupported SiNWs, and graphene, (d) comparison of the voltage profile of SiNW-G at various currents, and (e) is the cycle capability of SiNW-G at 6.8 A/g. (N.B. All capacities are based on the mass of silicon and graphene.)

structural changes that include reconstruction of the conjugate pi bonding leads to enhanced conductivity.[60] This is the reason that PAN was selected as an ideal binder in this work. To show this effect, we fabricated a cell using sodium salt of carboxy methyl cellulose (NaCMC) as a binder under the same conditions, although with elimination of the heat treatment step. This sample is labeled as c-SiNW-G-CMC, and its cycle performance shown in Figure 4b demonstrates that its performance gradually decreases in comparison to the sample with PAN.

Electrochemical cycling of c-SiNW-G by CV in Figure 5a illustrates a first cycle peak starting at 0.15 V corresponding to the cathodic lithiation of crystalline Si to form Li_xSi. The anodic peaks at 0.32 and 0.51 V correspond to the delithiation of Li_xSi back to Si. Subsequent cycles show an additional cathodic peak appearing at 0.20 V which becomes broader and stronger with each of the initial cycles. Together with the increasing strength of the anodic peaks at 0.32 and 0.51 V, these observations relate to a gradual activation of the SiNWs materials and a degradation of Si crystallinity with the alloying/dealloying mechanism. The impedance spectra (Figure 5b) for the lithium-ion cells were modeled using the equivalent circuit provided in Figure 5b (inset). In this circuit, R1 represents the contact resistance (or the electrode series resistance), R2 and R3 are the charge transfer resistances, CPE1 and CPE2 are the capacitances, and W is the Warburg diffusion resistance. A table of these calculated values is provided in Table S1 in the Supporting Information. The general trend is that the graphene-based lithium-ion cell has relatively lower contact resistance values, which likely arise because of the high conductivity of graphene. The carbon-coated SiNWs on graphene showed a synergistic enhancement of the perform-

dx.doi.org/10.1021/am5032067 | ACS Appl. Mater. Interfaces 2014, 6, 13757−13764

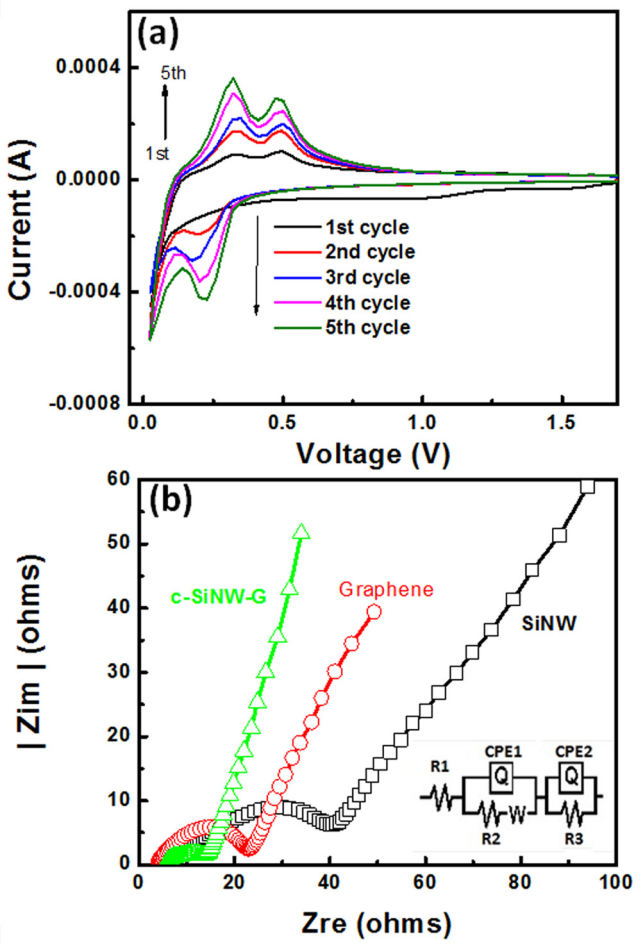

Figure 5. (a) Cyclic voltammogram for a coin cell fabricated using c-SiNW-G; (b) EIS for coin cells fabricated using c-SiNW-G, SiNWs, and graphene.

ance represented by the lowest charge transfer resistance. This may be attributed to the enhanced conductivity provided by the carbon coating throughout the entire 3D structure.

After cycling at high current density, the SiNW-G anodes were extracted from their assembly and rinsed to remove the electrolyte. This was done to image the structural retention of SiNWs and to investigate amorphization of the (111) crystal plane after cycling. As previously mentioned, crystallinity along the axis of the wire would promote diffusion and would support the excellent capacity retention and cycle durability at high current density. A fundamental study that monitored in situ lithiation/delithiation of SiNWs, noted stress occurs primarily at the Si−Si bond between the (111) planes during cycling, potentially leaving the crystal plane partial intact along the optimally oriented (111) nanowires.[29,50] As depicted by TEM microscopy in Figures 6a and 6b, there was a general retention of SiNWs morphology, despite significant fragmentation and swelling of the SiNWs. However, after the amorphization of Si and degradation during cycling, HRTEM imaging and the corresponding FFT of the SiNW-G composites in Figure 6c clearly shows no visible retention of crystallinity in the (111) plane. EDX mapping in Figure 6d−f confirms the entangled SiNWs within the body of the carbon composite. Further, the oxygen presence corresponds to the formation of SEI and residual electrolyte that was not removed after rinsing the electrodes.

In summary, we have developed a simple, one-pot synthesis methodology capable of growing bulk SiNWs on a low-cost NiNPs catalyst. Furthermore, we illustrated the potential for these NiNPs to be simultaneously anchored to three-dimensional support materials, enabling a large range of future application areas for this method of (111) SiNWs growth. After growing the carbon-coated c-SiNW-G composite, we were able to show its excellent durability and retention of capacity at high current density (100th cycle: 550 mAh g^{-1} @ 6.8 A g^{-1}) an anode in a LIB cell. Ultimately, this process creates an important building block for a new wave of low-cost, high-rate, silicon nanowire materials.

■ ASSOCIATED CONTENT

Supporting Information

Optical image of the electrode before and after annealing, cycle performance of c-SiNW-G in comparison with graphene for

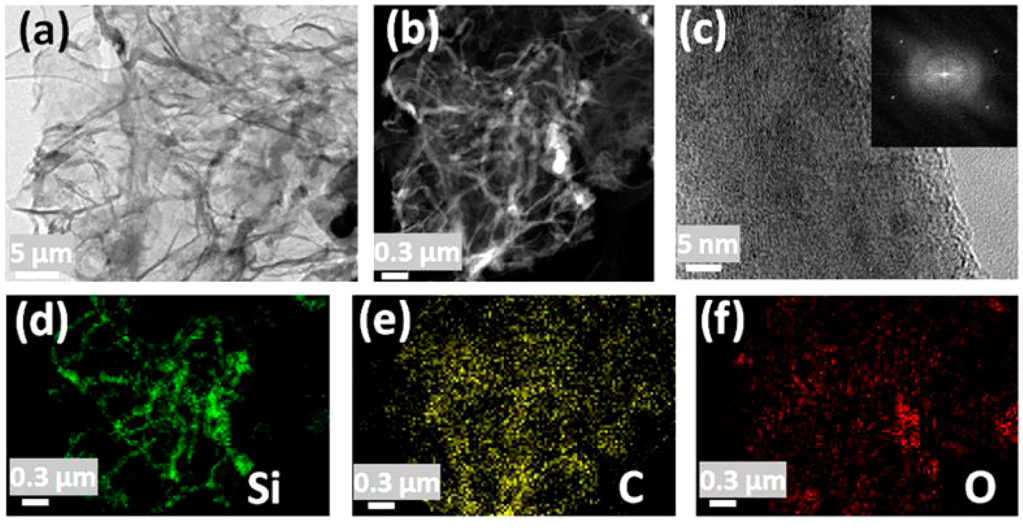

Figure 6. (a) TEM image for SiNW-G electrode material after 100 cycles. (b) HAADF-STEM, (c) HRTEM, and (d−f) EDX mapping for the elements silicon, carbon and oxygen, respectively, in SiNW-G after cycling.

100 cycles, and EIS modeling data. This material is available free of charge via the Internet at http://pubs.acs.org.

AUTHOR INFORMATION

Corresponding Authors

*E-mail: xingcheng.xiao@gm.com.
*E-mail: zhwchen@uwaterloo.ca.

Notes

The authors declare no competing financial interest.

ACKNOWLEDGMENTS

The authors would like to acknowledge financial support from the Natural Sciences and Engineering Research Council of Canada (NSERC), the University of Waterloo, and the Waterloo Institute for Nanotechnology. TEM and HAADF-STEM were obtained at the Canadian Center for Electron Microscopy (CCEM) located at McMaster University. X.C.X. also acknowledges the support by the Assistant Secretary for Energy Efficiency and Renewable Energy, Office of Vehicle Technologies of the U.S. Department of Energy under contract no. DE-AC02-05CH11231, subcontract no. 7056410 under the Batteries for Advanced Transportation Technologies (BATT) Program.

ABBREVIATIONS

CV, cyclic voltammetry
CD, galvanostatic charge−discharge
EIS, electrochemical impedance spectroscopy
EDX, energy-dispersive X-ray
HAADF-STEM, high-angle annular dark field scanning transmission electron micrograph
NiNPs, nickel nanoparticles
rGO, reduced graphene oxide
SEI, solid electrolyte interphase layer
SiNWs, silicon nanowires
SiNW-G SiNWs on rGO composite
c-SiNW-G, carbon-coated SiNWs on rGO composite
SEM, scanning electron micrograph
TEM, transmission electron micrograph
VLS, vapor−liquid−solid
VSS, vapor−solid−solid
XRD, X-ray powder diffraction

REFERENCES

(1) Hassan, F.; Chen, Z.; Yu, A.; Xaio, X. Sn/Sno$_2$ Embedded in Mesoporous Carbon Nanocomposites as Negative Electrode for Lithium Ion Batteries. *Electrochim. Acta* **2012**, *87*, 844−852.

(2) Liao, J.-Y.; Higgins, D.; Liu, G.; Chabot, V.; Xiao, X.; Chen, Z. Multifunctional TiO_2-C/MnO_2 Core-Double-Shell Nanowire Arrays as High-Performance 3d Electrodes for Lithium Ion Batteries. *Nano Lett.* **2013**, *13*, 5467−5473.

(3) Yu, A.; Park, H. W.; Davies, A.; Higgins, D.; Chen, Z.; Xaio, X. Free-Standing Layer-by-Layer Hybrid Thin Film of Graphene-MnO_2 Nanotube as Anode for Lithium Ion Batteries. *J. Phys. Chem. Lett.* **2011**, *2*, 1855−1860.

(4) Tarascon, J.-M.; Armand, M. Issues and Challenges Facing Rechargable Lithium Batteries. *Nature* **2001**, *414*, 359−367.

(5) Armand, M.; Tarascon, J.-M. Building Better Batteries. *Nature* **2008**, *451*, 652−657.

(6) Yu, Y.; Gu, L.; Zhu, C.; Tsukimoto, S.; Aken, P. A.; Maier, J. Reversible Storage of Lithium in Silver-Coated Three-Dimensional Macroporous Silicon. *Adv. Mater.* **2010**, *22*, 2247−2250.

(7) Kim, H.; Seo, M.; Park, M.-H.; Cho, J. A Critical Size of Silicon Nano-Anodes for Lithium Rechargable Batteries. *Angew. Chem., Int. Ed.* **2010**, *49*, 2146−2149.

(8) Sharma, R. A.; Seefurth, R. N. Thermodynamic Properties of the Lithium-Silicon System. *J. Electrochem. Soc.* **1976**, *123*, 1763−1768.

(9) Wu, H.; Cui, Y. Designing Nanostructured Si Anodes for High Energy Lithium Ion Batteries. *Nanotoday* **2012**, *7*, 414−429.

(10) Chan, C. K.; Peng, H.; Liu, G.; McIlwraith, K.; Zhang, X. F.; Huggins, R. A.; Cui, Y. High-Performance Lithium Battery Anodes Using Silicon Nanowires. *Nat. Nanotechnol.* **2008**, *3*, 31−35.

(11) Kim, H.; Han, B.; Choo, J.; Cho, J. Three-Dimensional Porous Silicon Particles for Use in High-Performance Lithium Secondary Batteries. *Angew. Chem., Int. Ed.* **2008**, *47*, 10151−10154.

(12) Besenhard, J. O.; Yang, J.; Winter, M. Will Advanced Lithium-Alloy Anodes Have a Chance in Lithium-Ion Batteries? *J. Power Sources* **1997**, *68*, 87−90.

(13) Raimann, P. R.; Hochgatterer, N. S.; Korepp, C.; Möller, K. C.; Winter, M.; Schröttner, H.; Hofer, F.; Besenhard, J. O. Monitoring Dynamics of Electrode Reactions in Li-Ion Batteries by in-Situ Esem. *Ionics* **2006**, *12*, 253−255.

(14) Beaulieu, L. Y.; Eberman, K. W.; Turner, R. L.; Krause, L. J.; Dahn, J. R. Colossal Reversible Volume Changes in Lithium Alloys. *Electrochem. Solid-State Lett.* **2001**, *4*, A137−140.

(15) Holzapfel, M.; Buga, H.; Scheifele, W.; Novak, P.; Petrat, F.-M. A New Type of Nano-Sized Silicon/Carbon Composite Electrode for Reversible Lithium Insertion. *Chem. Commun.* **2005**, *12*, 1566−1568.

(16) Wu, H.; Chan, G.; Choi, J. W.; Ryu, I.; Yao, Y.; McDowell, M. T.; Lee, S. E.; Jackson, A.; Yang, Y.; Hu, L.; Cui, Y. Stable Cycling of Double-Walled Silicon Nanotube Battery Anodes through Solid-Electrolyte Interphase Control. *Nat. Nanotechnol.* **2012**, *7*, 310−315.

(17) Kasavajjula, U.; Wang, C.; Appleby, A. J. Nano- and Bulk-Silicon-Based Insertion Anodes for Lithium-Ion Secondary Cells. *J. Power Sources* **2007**, *163*, 1003−1039.

(18) Ji, L.; Zhang, X. Evaluation of Si/Carbon Composite Nanofiber-Based Insertion Anodes for New-Generation Rechargeable Lithium-Ion Batteries. *Energy Environ. Sci.* **2010**, *3*, 124−129.

(19) Gómez Cámer, J. L.; Morales, J.; Sánchez, L.; Ruch, P.; Ng, S. H.; Kötz, R.; Novák, P. Nanosized Si/Cellulose Fiber/Carbon Composites as High Capacity Anodes for Lithium-Ion Batteries: A Galvanostatic and Dilatometric Study. *Electrochim. Acta* **2009**, *54*, 6713−6717.

(20) Liu, N.; Wu, H.; McDowell, M. T.; Yao, Y.; Wang, C.; Cui, Y. A Yolk-Shell Design for Stabilized and Scalable Li-Ion Battery Alloy Anodes. *Nano Lett.* **2012**, *12*, 3315−3321.

(21) Luo, J.; Zhao, X.; Wu, J.; Jang, H. D.; Kung, H. H.; Huang, J. Crumpled Graphene-Encapsulated Si Nanoparticles for Lithium Ion Battery Anodes. *J. Phys. Chem. Lett.* **2012**, *3*, 1824−1829.

(22) Zhou, X.; Yin, Y. X.; Wan, L. J.; Guo, Y. G. Facile Synthesis of Silicon Nanoparticles Inserted into Graphene Sheets as Improved Anode Materials for Lithium-Ion Batteries. *Chem. Commun.* **2012**, *48*, 2198−2200.

(23) Jang, S.-M.; Miyawaki, J.; Tsuji, M.; Mochida, I.; Yoon, S.-H. The Preparation of a Novel Si−Cnf Composite as an Effective Anodic Material for Lithium−Ion Batteries. *Carbon* **2009**, *47*, 3383−3391.

(24) Zhao, X.; Hayner, C. M.; Kung, M. C.; Kung, H. H. In-Plane Vacancy-Enabled High-Poweer Si-Grphene Composite Electrode for Lithium-Ion Batteries. *Adv. Energy Mater.* **2011**, *1*, 1079−1084.

(25) Lee, J. K.; Smith, K. B.; Hayner, C. M.; Kung, H. H. Silicon Nanoparticles-Graphene Paper Composites for Li Ion Battery Anodes. *Chem. Commun.* **2010**, *46*, 2025−2027.

(26) Tao, H.-C.; Fan, L.-Z.; Mei, Y.; Qu, X. Self-Supporting Si/Reduced Graphene Oxide Nanocomposite Films as Anode for Lithium Ion Batteries. *Electrochem. Commun.* **2011**, *13*, 1332−1335.

(27) Xin, X.; Zhou, X.; Wang, F.; Yao, X.; Xu, X.; Zhu, Y.; Liu, Z. A 3d Porous Architecture of Si/Graphene Nanocomposite as High-Performance Anode Materials for Li-Ion Batteries. *J. Mater. Chem.* **2012**, *22*, 7724−7730.

(28) Cui, L.-F.; Ruffo, R.; Chan, C. K.; Peng, H.; Cui, Y. Crystalline-Amorphous Core-Shell Silicon Nanowires for High Capacity and High Current Battery Electrodes. *Nano Lett.* **2009**, *9*, 491−495.
(29) Zhang, Q.; Cui, Y.; Wang, E. Anisotropic Lithium Insertion Behavior in Silicon Nanowires: Binding Energy, Diffusion Barrier, and Strain Effect. *J. Phys. Chem. C* **2011**, *115*, 9376−9381.
(30) Wang, X. L.; Han, W. Q. Graphene Enhances Li Storage Capacity of Porous Single-Crystalline Silicon Nanowires. *ACS Appl. Mater. Interfaces* **2010**, *2*, 3709−3713.
(31) Zhang, C.; Gu, L.; Kaskhedikar, N.; Cui, G.; Maier, J. Preparation of Silicon@Silicon Oxide Core-Shell Nanowires from a Silica Precursor toward a High Energy Density Li-Ion Battery Anode. *ACS Appl. Mater. Interfaces* **2013**, *5*, 12340−12345.
(32) Lee, S. E.; Kim, H. J.; Kim, H.; Park, J. H.; Choi, D. G. Highly Robust Silicon Nanowire/Graphene Core-Shell Electrodes without Polymeric Binders. *Nanoscale* **2013**, *5*, 8986−8991.
(33) Ge, M.; Rong, J.; Fang, X.; Zhang, A.; Lu, Y.; Zhou, C. Scalable Preparation of Porous Silicon Nanoparticles and Their Application for Lithium-Ion Battery Anodes. *Nano Res.* **2013**, *6*, 174−181.
(34) Wang, B.; Li, X.; Zhang, X.; Luo, B.; Zhang, Y.; Zhi, L. Contact-Engineered and Void-Involved Silicon/Carbon Nanohybrids as Lithium-Ion-Battery Anodes. *Adv. Mater.* **2013**, *25*, 3560−3565.
(35) Wu, Y.; Cui, Y.; Huynh, L.; Barrelet, C. J.; Bell, D. C.; Lieber, C. M. Controlled Growth and Structures of Molecular-Scale Silicon Nanowires. *Nano Lett.* **2004**, *4*, 433−436.
(36) Park, M.-H.; Kim, M. G.; Joo, J.; Kim, K.; Kim, J.; Ahn, S.; Cui, Y.; Cho, J. Silicon Nanotube Battery Anodes. *Nano Lett.* **2009**, *9*, 3844−3847.
(37) Hassan, F.; Chabot, V.; Elsayed, A. R.; Xiao, X.; Chen, Z. Engineered Si Electrode Nano-Architecture: A Scalable Treatment for the Production of Next-Generation Li-Ion Batteries. *Nano Lett.* **2014**, *14*, 277−283.
(38) Schmidt, V.; Wittemann, J. V.; Senz, S.; Gösele, U. Silicon Nanowires: A Review on Aspects of Their Growth and Their Electrical Properties. *Adv. Mater.* **2009**, *21*, 2681−2702.
(39) Song, T.; Xia, J.; Lee, J.-H.; Lee, D. H.; Kwon, M.-S.; Choi, J.-M.; Wu, J.; Doo, S. K.; Chang, H.; Park, W. I.; Zang, D. S.; Kim, H.; Huang, Y.; Hwang, K.-C.; Rogers, J. A.; Paik, U. Arrays of Sealed Silicon Nanotubes as Anodes for Lithium Ion Batteries. *Nano Lett.* **2010**, *10*, 1710−1716.
(40) Morales, A. M.; Lieber, C. M. A Laser Ablation Method for the Synthesis of Crystalline Semiconductor Nanowires. *Science* **1998**, *279*, 208−211.
(41) Givarigizov, E. I. Fundamentals Aspects of Vls Growth. *J. Cryst. Growth* **1975**, *31*, 20−30.
(42) Wagner, R. S.; Ellis, W. C. Vapor-Liquid-Solid Mechanism of Single Crystal Growth. *Appl. Phys. Lett.* **1964**, *4*, 89.
(43) Chabot, V.; Feng, K.; Park, H. W.; Hassan, F.; Elsayed, A. R.; Yu, A.; Xiao, X.; Chen, Z. Graphene Wrapped Silicon Nanocomposites for Enhanced Electrochemical Performance in Lithium Ion Batteries. *Electrochim. Acta* **2014**, *130*, 127−134.
(44) Zhang, Y.; Zhang, Q.; Wang, N.; Yan, Y.; Huihua, Z.; Zhu, J. Synthesis of Thin Si Whiskers (Nanowires) Using Sicl4. *J. Cryst. Growth* **2001**, *226*, 185−191.
(45) Ren, J. G.; Wang, C.; Wu, Q. H.; Liu, X.; Yang, Y.; He, L.; Zhang, W. A Silicon Nanowire-Reduced Graphene Oxide Composite as a High-Performance Lithium Ion Battery Anode Material. *Nanoscale* **2014**, *6*, 3353−3360.
(46) Léonard, F.; Talin, A. A. Electrical Contacts to One- and Two-Dimensional Nanomaterials. *Nat. Nanotechnol.* **2011**, *6*, 773−783.
(47) Dellas, N. S.; Liu, B. Z.; Eichfield, S. M.; Mayer, T. S.; Mohney, S. E. Orientation Dependance of Nickel Silicide Formation in Contacts to Silicon Nanowires. *J. Appl. Phys.* **2009**, *105*, 094309.
(48) Nash, P.; Nash, A. The Ni-Si (Nickel-Silicon) System. *Bull. Alloy Phase Diagrams* **1987**, *9*, 6−14.
(49) Hummers, W. S.; Offeman, R. E. Preparation of Graphitic Oxide. *J. Am. Chem. Soc.* **1958**, *80*, 1339−1339.
(50) Lee, S. W.; McDowell, M. T.; Choi, J. W.; Cui, Y. Anomalous Shape Changes of Silicon Nanopillars by Electrochemical Lithiation. *Nano Lett.* **2011**, *11*, 3034−3039.
(51) Machado, B. F.; Serf, P. Graphene-Based Materials for Catalysis. *Catal. Sci. Technol.* **2012**, *2*, 54−75.
(52) Chabot, V.; Higgins, D.; Yu, A.; Xiao, X.; Chen, Z.; Zhang, J. A Review of Graphene and Graphene Oxide Sponge: Material Synthesis and Applicatons to Energy and the Environment. *Energy Environ. Sci.* **2014**, *7*, 1564−1596.
(53) Kingma, K. J.; Hemley, R. J. Raman Spectroscopic Study of Microcrystalline Silica. *Am. Mineral.* **1994**, *79*, 269−273.
(54) Karakassides, M. A.; Gournis, D.; Petridis, D. An Infrared Reflectance Study of Si-O Vibrations in Thermally Treated Alkali-Saturated Montmorillonites. *Clay Miner* **1999**, *34*, 429−438.
(55) Ferrari, A. C. Raman Spectroscopy of Graphene and Graphite: Disorder, Electron−Phonon Coupling, Doping and Nonadiabatic Effects. *Solid State Commun.* **2007**, *143*, 47−57.
(56) Ferrari, A. C.; Meyer, J. C.; Scardaci, V.; Casiraghi, C.; Lazzeri, M.; Mauri, F.; Piscanec, S.; Jiang, D.; Novoselov, S. R.; Geim, A. K. Raman Spectrum of Graphene and Graphene Layers. *Phys. Rev. Lett.* **2006**, *97*, 187401.
(57) Zou, Y. Q.; Wang, Y. NiO Nanosheets Grown on Graphene Nanosheets as Superior Anode Materials for Li-Ion Batteries. *Nanoscale* **2011**, *3*, 2615−2620.
(58) Guo, P.; Song, H.; Chen, X. Electrochemical Performance of Graphene Nanosheets as Anode Material for Lithium-Ion Batteries. *Electrochem. Commun.* **2009**, *11*, 1320−1324.
(59) Pan, D.; Wang, S.; Zhao, B.; Wu, M.; Zhang, H.; Wang, Y.; Jiao, Z. Li Storage Properties of Disordered Graphene Nanosheets. *Chem. Mater.* **2009**, *21*, 3136−3142.
(60) Rahaman, M. S. A.; Ismail, A. F.; Mustafa, A. A Review of Heat Treatment on Polyacrylonitrile Fiber. *Polym. Degrad. Stab.* **2007**, *92*, 1421−1432.

NOTE ADDED AFTER ASAP PUBLICATION

This paper was published on the Web on August 7, 2014. Additional text and graphic changes were made throughout the paper, and the corrected version was reposted on August 13, 2014.